coatings

MDPI

Article

Macroparticle Reduction and Its Transport Mechanism through a Magnetic Filter during Cathodic Vacuum Arc Deposition with an HEA Target

Pei-En Lee [1], Yu-Kuan Tu [1], Ming-Hung Tsai [2,3], Che-Wei Tsai [1,2,*] and Jien-Wei Yeh [1,2,*]

[1] Department of Materials Science and Engineering, National Tsing Hua University, Hsinchu 30013, Taiwan
[2] High Entropy Materials Center, National Tsing Hua University, Hsinchu 30013, Taiwan
[3] Department of Materials Science and Engineering, National Chung Hsing University, 250 Kuo Kuang Road, Taichung 40227, Taiwan
* Correspondence: chewei@mx.nthu.edu.tw (C.-W.T.); jwyeh@mx.nthu.edu.tw (J.-W.Y.); Tel.: +886-3-5715131 (ext. 35370) (C.-W.T.); +886-3-5719558 (J.-W.Y.); Fax: +886-3-5722366 (J.-W.Y.)

Abstract: By cathodic arc deposition, the effects of the magnetic field, working pressure, inner-wall structure, and cross-section area of the magnetic-filter duct on the macroparticle (MP) distribution were investigated with a high-entropy alloy target. The MP density increased with the density of the plasma beam transporting through the filter duct, which was increased by the magnetic field or working pressure. In order to reduce the MP density, equally spaced circumferential Cu-sheet baffle and lining of 304-stainless-steel wire mesh were used as the inner-wall structure, respectively, but the improvement was limited. However, inserting an Al foil disk with a round opening for the passage of the main plasma stream at the bend position of the duct remarkably reduced the area fraction of the MPs from 4.8% to 0.6%. These results demonstrate that the main transport mechanism of the MPs was the entrainment in the plasma beam through the duct. In addition, reducing the cross section of the filter duct was suggested to be an effective method to reduce MPs. This method could be utilized for high-MP generation targets such as high-entropy alloys.

Keywords: PVD; cathodic arc deposition; macroparticles; droplet; magnetic filter

check for updates

Citation: Lee, P.-E.; Tu, Y.-K.; Tsai, M.-H.; Tsai, C.-W.; Yeh, J.-W. Macroparticle Reduction and Its Transport Mechanism through a Magnetic Filter during Cathodic Vacuum Arc Deposition with an HEA Target. *Coatings* **2022**, *12*, 1437. https://doi.org/10.3390/coatings12101437

Academic Editor: Christian Mitterer

Received: 2 September 2022
Accepted: 28 September 2022
Published: 29 September 2022

1. Introduction

Cathodic vacuum arc deposition (CVAD) has been widely used for cutting tools in the coating industry, since it contributes to a high deposition rate and strong adhesion between a film and substrate [1]. However, the cathodic arc emits metal droplets from the target, often referred to as macroparticles (MPs) [2,3]. They are generally in the range of 0.1–10 μm, depending on the cathode material and deposition parameters [4]. The MPs cause defects in films, deteriorating the microstructure and mechanical properties. This slows the development of CVAD in optics and microelectronics. Therefore, the suppression of MPs has been the subject of numerous investigations [5]. Generally, the plasma can be guided by a magnetic coil to retard the MPs on films, since the larger MPs tend to deposit on the duct wall [6,7]. In this case, much research has focused on improving the plasma transmission efficiency using different duct structures [8]. However, the MPs still cannot be removed by the magnetic filter systems completely.

Until now, there has been limited research on the further reduction in MP density and the transport mechanism of MPs in magnetic filter systems. Three mechanisms of MP transport have been proposed [9–11]. The MPs can be transported through the filter duct by mechanical bouncing, electrostatic reflection, and entrainment in plasma. However, few experimental results have confirmed which mechanism is most effective, so the appropriate mechanism is still unclear.

The four effects of HEA, which are the high entropy effect, lattice distortion effect, slow diffusion effect, and the cocktail effect [12], give HEA particular properties that can be widely used in a variety of applications. In consideration of the high efficiency of CVAD and the promising performances of high-entropy alloy coatings including alloy films [13–19], nitride films [12,20–25], and carbide films [26,27] produced by the magnetic sputtering method, the present work studied the films by CVAD from a one-piece target of a high-entropy alloy. The influence of the magnetic field and the working pressure on the deposition rate and MP density was investigated. The relationship between the distribution of MPs and the plasma density at the duct exit was analyzed. In addition, different structures on the duct wall and a reduced cross-section area of the duct were investigated to determine their abilities to reduce the MP density and to confirm the real mechanism of MP transport.

2. Materials and Methods

A schematic diagram of the experimental apparatus is shown in Figure 1. An $Al_{0.5}CoCrCu_{1.5}FeNi$ high-entropy alloy target, which was 15 mm thick and 100 mm in diameter, was used as cathode. It was produced by arc melting in a water-cooled copper crucible and casting in ceramic shell mold. The $Al_{0.5}CoCrCu_{1.5}FeNi$ nitride films were deposited on (100) Si wafers with a background pressure below 3×10^{-5} Torr. All experiments were conducted with 70 A arc current, −50 V substrate bias, and a 50% N_2 flow ratio of Ar + N_2. The magnetic filter duct was a bent pipe with an inner diameter of 190 mm and a bend angle of 90°. The distance from the exit of the filter duct to the substrate surface was 5 cm. The magnitudes of magnetic fields of 0, 180, 224, and 292 G were applied on the filter duct to determine the influence of the magnetic field on MP density under the working pressure of 10 mtorr. The working pressures of 5, 10, 20 mtorr was also used to observe the differences on MP density on the films deposited under a 224 G magnetic field.

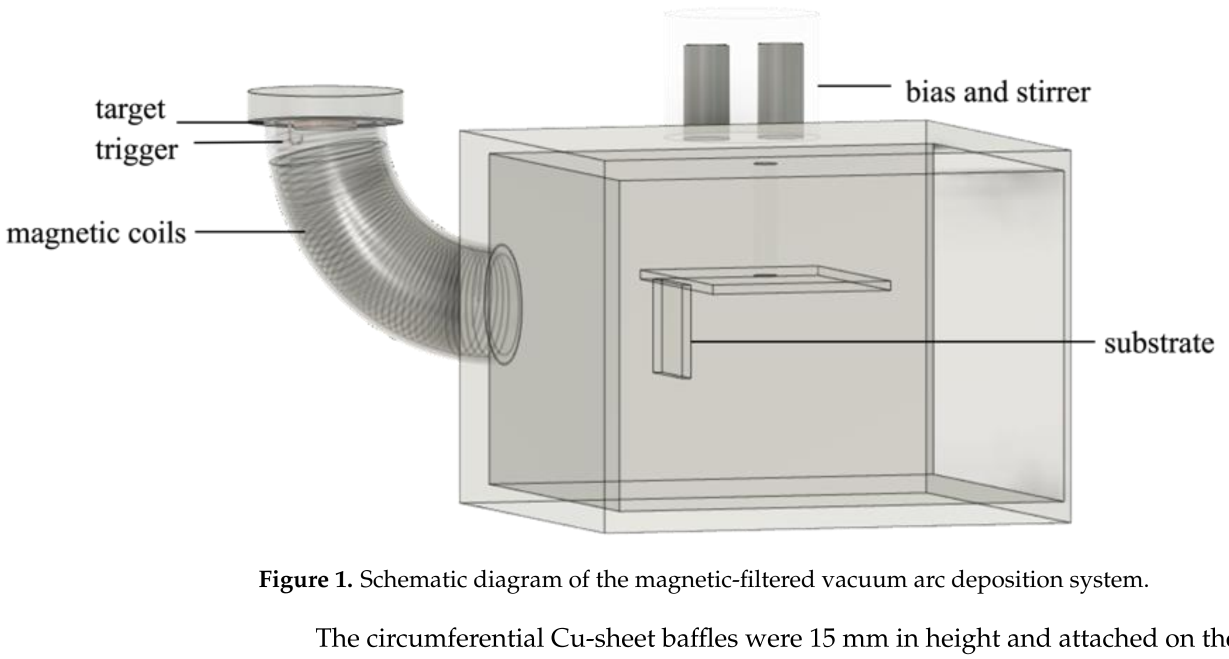

Figure 1. Schematic diagram of the magnetic-filtered vacuum arc deposition system.

The circumferential Cu-sheet baffles were 15 mm in height and attached on the inner wall with an equal spacing of 50 mm from the target to the substrate along the duct. A lining of 100-mesh 304-stainless-steel wire mesh on the inner wall was also used. This were designed to change the inner structure of the magnetic-filter duct for capturing MPs, as shown in Figure 2a,b, to reduce the MP density under the deposition condition with a 224 G magnetic field and a working pressure of 10 mtorr. Moreover, the area of the filter duct cross section was reduced by inserting an 8-μm thick Al foil disk at the bend position to provide a round opening, as shown in Figure 2c. The hole was 90 mm in diameter and centered at a distance 30 mm from the disk center. The effect of area reduction was investigated with the deposition under 10 mtorr of working pressure and a 224 G magnetic field.

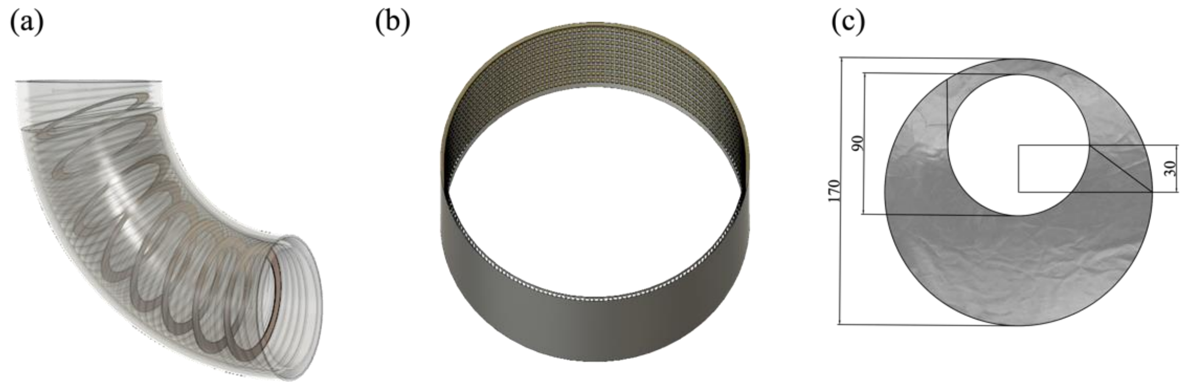

Figure 2. Magnetic-filter duct (**a**) lined with Cu-sheet baffles, (**b**) lined with 304 SS wire meshes along the length of duct, (**c**) with an Al foil inserted at the bend position to provide a round opening.

The microstructure of the thickness and surface morphology was analyzed by SEM (JEOL JSM 6500F). The density and dimension of the MPs were observed with SEM and calculated by an image analysis system. Several SEM images were taken at low magnification on our films randomly. Then, image J was adopted to calculate the number and diameters of the MPs, and we used the average [28].

3. Results

3.1. The Effect of the Magnetic Field and Working Pressure on the Filter Duct

The deposition rate and substrate current as a function of the magnetic field of the filter duct from the experimental high-entropy target are shown in Figure 3. The substrate current and the deposition rate increased with the increase in the magnetic field. This reflects that the plasma density arriving at the substrate was increased and more ions and electrons were restrained in the plasma beam by a higher magnetic force, which meant that more ions would spiral through the filter duct to be deposited on the substrate. Similar results were also observed in previous research [10]. It also revealed that the films were not formed on the Si substrate when the magnetic field was 0 G. This reflects no plasma beam formed under 0 G.

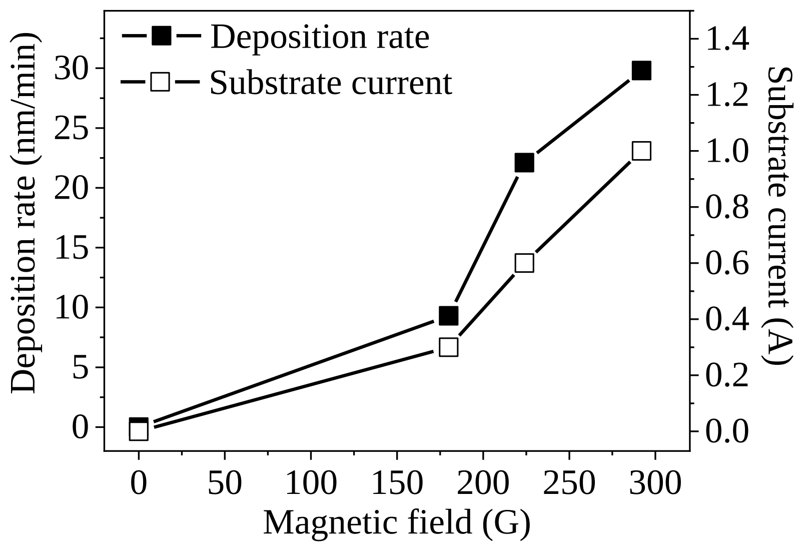

Figure 3. Deposition rate and substrate current as functions of the magnetic field.

The distribution of MP density under different magnetic fields of the filter duct is shown in Figure 4. The largest population of MPs was in the range of 0.5 to 1 µm. The MP density increased with the increasing magnetic field and thus increasing plasma density.

A large increase in MPs was found as the magnetic field increased from 224 to 292 G. In addition, few MPs were found on the substrate when the magnetic field was 0 G.

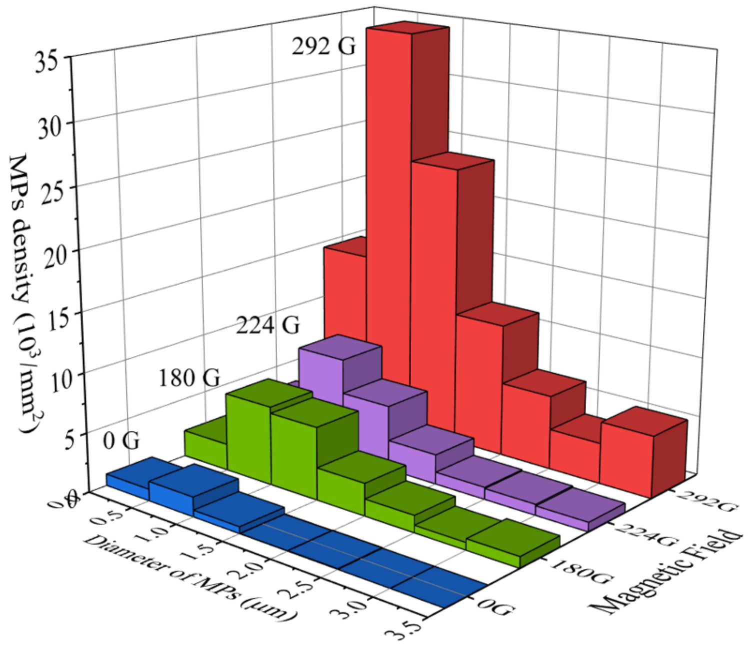

Figure 4. Distributions of MP density under different magnetic fields: (a) 0 G; (b) 180 G; (c) 224 G; and (d) 292 G.

The dependence of the deposition rate and substrate current on the working pressure is shown in Table 1. The substrate current and deposition rate decreased with the increase in working pressure. This is due to the fact that there were more collisions between ions and gas molecules at a higher working pressure. The ions might possess a lower charge state or depart from the moving path of the plasma after their collisions with gas molecules [29].

Table 1. Deposition rate and substrate current for different working pressures.

Working Pressure (mtorr)	Deposition Rate (nm/min)	Substrate Current (A)
5	28.5	1.8
10	22.1	0.6
20	9.7	0.3

The distribution of MP density at different working pressures is shown in Figure 5. The films deposited under lower pressure displayed a higher MP density. As shown in Table 1 and Figure 5, with a decrease in the working pressure, the plasma density arriving at the substrate was higher, and slightly more MPs were deposited on the films. Based on the results above, adjusting the magnetic field or the working pressure did not improve the MP density. Due to the slight effect of the deposition conditions, the change in direction provided by different structures of filter duct were studied.

3.2. *Effects of Different Inner Wall Structures and the Reduced Cross Section of the Duct on the MP Density*

In order to remove the MP transport through the filter duct by mechanical bouncing on the duct wall or electrostatic reflection near the duct wall, two kinds of inner wall structure were used to assess their effects. We prepared an attachment of circumferential Cu-sheet baffles and a lining of 304-stainless-steel wire mesh on the inner wall along the duct. On the other hand, we inserted an Al foil disk near the exit to provide a round opening for the plasma beam to pass through. In order to tally the center of the hole with the center of the plasma beam, a blind Al foil disk at the bend position was pierced by the plasma beam during an arcing and depositing condition to form a through-hole about 60 mm in diameter. This hole became the base to align the position of the artificial passage. The cross-section area of the hole was 64 cm^2, which was 28% of the filter duct with an area of 227 cm^2.

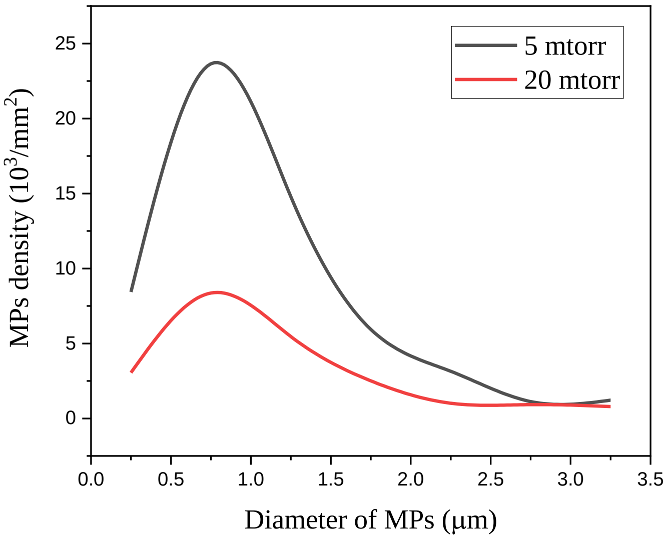

Figure 5. Distribution of MP density with different working pressures: (a) 5 mtorr and (b) 20 mtorr.

The distributions of MP density with different inner wall structures and the cross-section area of the duct are shown in Figures 6 and 7. The sample that was deposited under the condition of the magnetic filter duct without a lining had a 2.1% area fraction of MPs, whereas the one with the baffle lining and with the screen lining had 2.7% and 1.8%, respectively. This indicated that the MP density could not be reduced by different inner wall structures since the area fraction of the MPs varied between 1.8% and 2.7% without a decreasing trend. The increased number of smaller MPs in the distributions obtained with the baffle lining and wire mesh lining might be the result of their interference on the magnetic field in the filter duct.

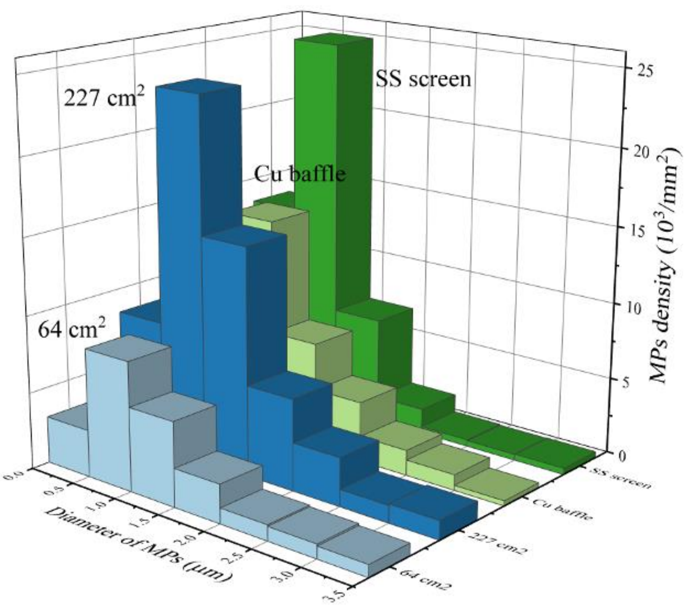

Figure 6. Distribution of MP density with different inner wall structures and different cross-section areas of 227 and 64 cm^2.

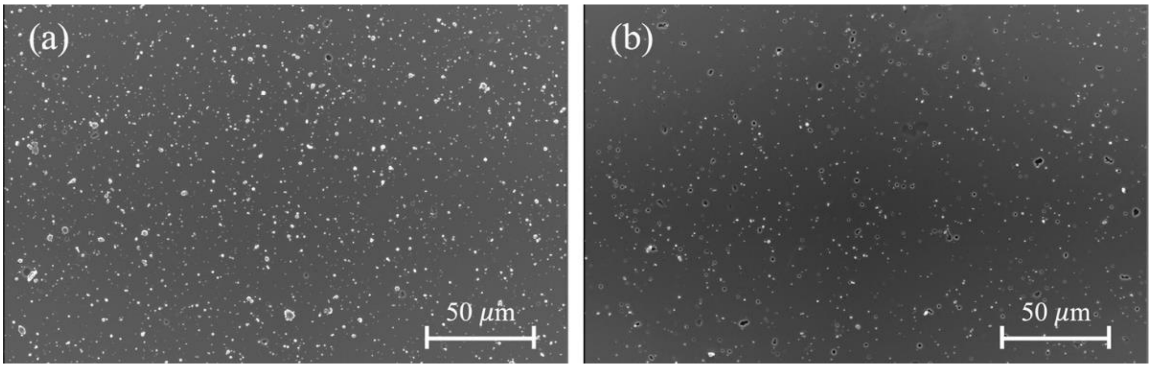

Figure 7. SEM plane-view images of deposited films obtained with different cross-section areas: (**a**) 227 cm^2 and (**b**) 64 cm^2.

On the other hand, the distributions of the MP density before and after reducing the cross-section area shown in Figures 6 and 7 demonstrates that the MP density greatly decreased when the cross-section area was reduced. The area fraction of the MPs, deposition rate, and substrate current is presented in Table 2. The area fraction of the MPs was remarkably decreased from 4.8% to 0.6%. The small loss in substrate current and deposition rate was due to the fact that the outer ions of plasma beam which could not pass through the hole directly deposited on the Al foil. This demonstrates that the reduction in the passage cross section was very effective in reducing MPs.

Table 2. Area fraction of MP density, deposition rate, and substrate current with different cross-section areas.

Cross-Section Area of Filter Duct (cm^2)	Area Fraction of MPs (%)	Deposition Rate (nm/min)	Substrate Current (A)
227	4.8	28.5	1.8
64	0.6	18.8	1.5

3.3. Relationship between MP Density and Plasma Density Distributions

Figure 8 presents the spatial relation between the MP density and plasma density distributions, in which a 100-mm diameter Si wafer was placed at the exit of the filter duct and centered at the maximum intensity of the plasma beam predetermined by depositing the film on a glass substrate. The Si wafer was divided into nine regions in whose center the film thickness and MP density distribution were measured. The film thickness distribution and the corresponding plasma distribution are shown in Figure 8. It can be seen in Figure 8b, the plasma density was highest at the center of Si wafer and had a larger spread in the direction of the periphery of the larger duct radius. This kind of distribution was typical and reported in previous research. It is attributable to the effect of centrifugal force [29].

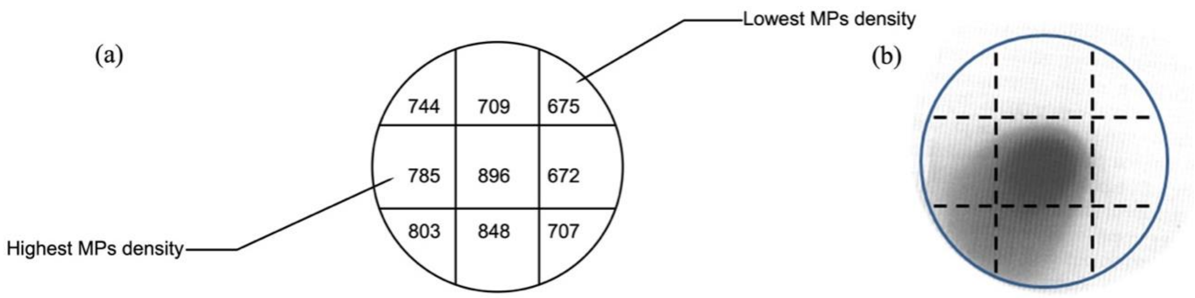

Figure 8. Schematic diagram of an Si wafer showing (**a**) the distribution of the film thickness and (**b**) corresponding plasma density distribution.

The fact that the highest MP density occurred at the left side of Si wafer indicated that the center of the MP density distribution was displaced to the left of the plasma center. The slight offset is explained later by the entrainment mechanism. In addition, the MP density had a radial distribution similar to that of the plasma density. This similar radial distribution suggested that the transportation of MPs through the duct had a close relation to the plasma beam.

4. Discussion

4.1. Transport Mechanism of MPs in the Filter Duct

Three mechanisms of MP transport have been proposed in previous research [9]: (i) mechanical bouncing on the duct wall; (ii) electrostatic reflection near the duct wall; and (iii) entrainment in the plasma beam. However, the actual mechanism was still unclear, since few experiments have been conducted to verify which mechanism is dominant. In this section, we explain the mechanism of entrainment with the present experimental results.

There are three reasons why the mechanism of mechanical bouncing on the duct wall and the mechanism of electrostatic reflection near the duct wall were mainly excluded. First, the utilization of baffle and screen-lining could not reduce the MP density. If the mechanical bouncing mechanism were true, the baffle would reflect a portion of the MPs, and the open holes in the screen would trap a portion of the MPs. The MPs were negatively charged by mobile electrons, and the plasma sheath on duct wall made it negatively biased [11]. Thus, the MPs were repelled by the electrostatic field when they passed through the duct and travelled toward the duct exit. Therefore, secondly, if the mechanical bouncing and electrostatic reflection mechanisms were true, the mechanical bouncing and electrostatic reflection should have enabled the MPs to jump and deposit onto the substrate by successive bouncing or reflection even when the magnetic field was 0 G. However, not only was no film deposited but few MPs were deposited on the substrate under 0 G magnetic field. Finally, if these two mechanisms could operate with the duct wall, they should also operate with the negatively biased substrate. That means MPs should bounce or reflect away from the substrate surface during ion deposition, and no MPs could attach to the substrate. Nevertheless, a significant number of MPs appeared on the films. Therefore, mechanical bouncing and electrostatic reflection are not the major mechanism of MP transport.

On the other hand, from the experimental results presented above: the MP density increased with the plasma density when the magnetic field was increased and the working pressure was decreased; and the MP density had a radial distribution similar to that of the plasma density. It can be concluded that the MPs transported through the filter duct by entrainment in plasma. Figure 9 shows the entrainment mechanism in which the MPs collide with the ions and are driven by ions to entrain the plasma beam, because each ion advances in a spiral motion around the magnetic line. This is similar to a sandstorm in which the sand particles are driven by air molecules to entrain the storm. As a result of the entrainment mechanism, more MPs can be transported if the plasma density and thus the deposition rate are increased, such as in the case of the increased magnetic field and decreased working pressure. As for the small deviation of the MPs center from that of the plasma density, this can be expected since the plasma beam is guided by the magnetic field, but the MPs are driven by the plasma beam. The different driving forces cause different centering.

4.2. The Merits of Using a Smaller Passage in the Midway of the Duct

The finding that a reduction in the passage cross section in the midway effectively reduced MPs can be explained with the space change during MP transportation. As the passage had an area around 28% of the total cross-section area of the duct, it can be expected that around 28% of MPs would pass through the passage and spread out again along the distance from the reduced passage to the exit. The dilution is equivalent to 28% to a first approximation. This is of the same order in the area fraction change of MPs from 4.8% to 0.6% (dilution ~12.5%). The discrepancy is reasonable since the estimation assumes that the MPs uniformly distribute in the cross section. Instead, the MP distribution has a center near the center of plasma beam and has a similar radial spread to that of the plasma beam. In addition, its spread is larger than that of the plasma beam because the MPs are driven by the ions of the plasma beam. Therefore, the calculation is reasonable but overestimated.

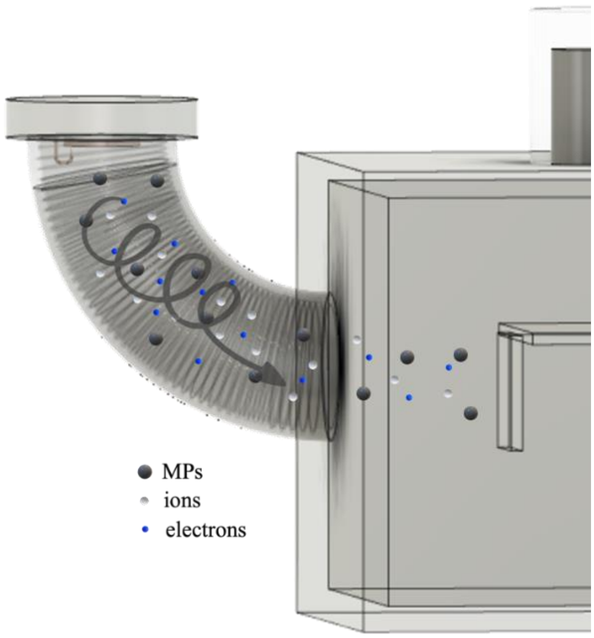

Figure 9. Schematic diagram showing the entrainment mechanism of MP transport.

It can be seen from Table 1 that the reduction in the passage cross section in the midway did not cause a large decrease in deposition rate. The reduced passage retained 66% of the deposition rate. This is due to the fact that the plasma beam is more concentrated than the MP flow, which has a larger ability to spread under the numerous collisions with the ions in the plasma beam. Despite the decrease in deposition rate, it produced a better structure of the films. Therefore, the reduced passage in the midway of the duct is an effective method in terms of quality and deposition rate.

5. Conclusions

The films by CVAD from the one-piece high-entropy alloy target were studied for the effect of the magnetic field, working pressure, different structures of duct wall, and cross-section area of the passage. The MP density on the films increased with the plasma density when the magnetic field was increased or the working pressure was decreased. Few MPs and no film were found on the substrate surface under a 0 G magnetic field. Both applications of baffle and screen lining on the duct wall slightly reduced the MP density. With a reduced passage in the midway of the filter duct, the area fraction of MPs was more effectively reduced from 4.8% to 0.6% than with the previous methods.

The experimental results excluded the mechanical bouncing and electrostatic reflection mechanisms but confirmed the entrainment mechanism for MP transportation in plasma. The entrainment mechanism suggests that the magnetic filter system still provides a way to transport MPs by plasma and deposit MPs on the films. However, the present work has found that inserting a smaller passage in the midway of the duct is an effective method in reducing the MPs without a large decrease in the deposition rate. In addition, the proposed method to reduce MPs would be important when using high-MP generation targets such as high-entropy alloys, which inherently have low thermal and electrical conductivity.

Author Contributions: Conceptualization, Y.-K.T.; methodology, Y.-K.T.; validation, Y.-K.T., P.-E.L.; formal analysis, Y.-K.T.; investigation, Y.-K.T. and M.-H.T.; resources, C.-W.T. and J.-W.Y.; data curation, Y.-K.T., M.-H.T. and P.-E.L.; writing—original draft preparation, Y.-K.T. and P.-E.L.; writing—review and editing, C.-W.T. and J.-W.Y.; visualization, P.-E.L.; supervision, C.-W.T. and J.-W.Y.; project administration, C.-W.T. and J.-W.Y.; funding acquisition, C.-W.T. and J.-W.Y. All authors have read and agreed to the published version of the manuscript.

Funding: This research received no external funding.

Institutional Review Board Statement: Not applicable.

Informed Consent Statement: Not applicable.

Data Availability Statement: Not applicable.

Acknowledgments: This work was financially supported by the "High Entropy Materials Center" from The Featured Areas Research Center Program within the framework of the Higher Education Sprout Project by the Ministry of Education (MOE) and from the Project NSTC 111-2634-F-007-008 - by the National Science and Technology Council (NSTC) in Taiwan.

Conflicts of Interest: The authors declare no conflict of interest.

References

1. Sanders, D.M.; Boercker, D.B.; Falabella, S. Coating technology based on the vacuum arc-a review. *IEEE Trans. Plasma Sci.* **1990**, *18*, 883–894. [CrossRef]
2. Swift, P. Macroparticles in films deposited by steered cathodic arc. *J. Phys. D Appl. Phys.* **1996**, *29*, 2025. [CrossRef]
3. Tai, C.; Koh, E.; Akari, K. Macroparticles on TiN films prepared by the arc ion plating process. *Surf. Coat. Technol.* **1990**, *43*, 324–335. [CrossRef]
4. Ali, M.; Hamzah, E.; Abbas, T.; Mohd Radzi, H.J.; Mohd, T.; Qazi, I.A. Macrodroplet reduction and growth mechanisms in cathodic arc physical vapor deposition of tin films. *Surf. Rev. Lett.* **2008**, *15*, 653–659. [CrossRef]
5. Anders, S.; Anders, A.; Brown, I. Macroparticle-free thin films produced by an efficient vacuum arc deposition technique. *J. Appl. Phys.* **1993**, *74*, 4239–4241. [CrossRef]
6. Miernik, K.; Walkowicz, J.; Bujak, J. Design and performance of the microdroplet filtering system used in cathodic arc coating deposition. *Plasmas Ions* **2000**, *3*, 41–51. [CrossRef]
7. Boxman, R.L.; Zhitomirsky, V.; Alterkop, B.; Gidalevich, E.; Beilis, I.; Keidar, M.; Goldsmith, S. Recent progress in filtered vacuum arc deposition. *Surf. Coat. Technol.* **1996**, *86*, 243–253. [CrossRef]
8. Aksenov, I.I.; Strel'Nitskij, V.E.; Vasilyev, V.V.; Zaleskij, D.Y. Efficiency of magnetic plasma filters. *Surf. Coat. Technol.* **2003**, *163*, 118–127. [CrossRef]
9. Boxman, R.L.; Goldsmith, S.; Ben-Shalom, A.; Kaplan, L.; Arbilly, D.; Gidalevich, E.; Zhitomirsky, V.; Ishaya, A.; Keidar, M. Filtered vacuum arc deposition of semiconductor thin films. *IEEE Trans. Plasma Sci.* **1995**, *23*, 939–944. [CrossRef]
10. Keidar, M.; Beilis, I.I.; Aharonov, R.; Arbilly, D.; Boxman, R.L.; Goldsmith, S. Macroparticle distribution in a quarter-torus plasma duct of a filtered vacuum arc deposition system. *J. Phys. D-Appl. Phys.* **1997**, *30*, 2972–2978. [CrossRef]
11. Keidar, M.; Beilis, I.I.; Boxman, R.L.; Goldsmith, S. Transport of macroparticles in magnetized plasma ducts. *IEEE Trans. Plasma Sci.* **1996**, *24*, 226–234. [CrossRef]
12. Chen, T.K.; Shun, T.T.; Yeh, J.W.; Wong, M.S. Nanostructured nitride films of multi-element high-entropy alloys by reactive DC sputtering. *Surf. Coat. Technol.* **2004**, *188*, 193–200. [CrossRef]
13. Lindfors, P.A.; Mularie, W.M.; Wehner, G.K. Cathodic arc deposition technology. *Surf. Coat. Technol.* **1986**, *29*, 275–290. [CrossRef]
14. Randhawa, H. Cathodic arc plasma deposition technology. *Thin Solid Film.* **1988**, *167*, 175–186. [CrossRef]
15. Randhawa, H.; Johnson, P. A review of cathodic arc plasma deposition processes and their applications. *Surf. Coat. Technol.* **1987**, *31*, 303–318. [CrossRef]
16. Feng, X.; Tang, G.; Sun, M.; Ma, X.; Wang, L.; Yukimura, K. Structure and properties of multi-targets magnetron sputtered ZrNbTaTiW multi-elements alloy thin films. *Surf. Coat. Technol.* **2013**, *228*, S424–S427. [CrossRef]
17. Chen, Y.; Munroe, P.; Xie, Z.; Zhang, S. High-entropy alloy-based coatings: Microstructures and properties. In *Protective Thin Coatings Technology*; CRC Press: Boca Raton, FL, USA, 2021; pp. 205–232.
18. Zhang, W.; Liaw, P.K.; Zhang, Y. Science and technology in high-entropy alloys. *Sci. China Mater.* **2018**, *61*, 2–22. [CrossRef]
19. Sha, C.; Zhou, Z.; Xie, Z.; Munroe, P. High entropy alloy FeMnNiCoCr coatings: Enhanced hardness and damage-tolerance through a dual-phase structure and nanotwins. *Surf. Coat. Technol.* **2020**, *385*, 125435. [CrossRef]
20. Chang, H.W.; Huang, P.K.; Yeh, J.W.; Davison, A.; Tsau, C.H.; Yang, C.C. Influence of substrate bias, deposition temperature and post-deposition annealing on the structure and properties of multi-principal-component (AlCrMoSiTi) N coatings. *Surf. Coat. Technol.* **2008**, *202*, 3360–3366. [CrossRef]
21. Lai, C.H.; Lin, S.J.; Yeh, J.W.; Chang, S.Y. Preparation and characterization of AlCrTaTiZr multi-element nitride coatings. *Surf. Coat. Technol.* **2006**, *201*, 3275–3280. [CrossRef]

22. Lai, C.H.; Lin, S.J.; Yeh, J.W.; Davison, A. Effect of substrate bias on the structure and properties of multi-element (AlCrTaTiZr) N coatings. *J. Phys. D Appl. Phys.* **2006**, *39*, 4628. [CrossRef]
23. Lai, C.H.; Cheng, K.H.; Lin, S.J.; Yeh, J.W. Mechanical and tribological properties of multi-element (AlCrTaTiZr) N coatings. *Surf. Coat. Technol.* **2008**, *202*, 3732–3738. [CrossRef]
24. Feng, X.; Tang, G.; Ma, X.; Sun, M.; Wang, L. Characteristics of multi-element (ZrTaNbTiW) N films prepared by magnetron sputtering and plasma based ion implantation. *Nucl. Instrum. Methods Phys. Res. Sect. B Beam Interact. Mater. At.* **2013**, *301*, 29–35. [CrossRef]
25. Sha, C.; Zhou, Z.; Xie, Z.; Munroe, P. FeMnNiCoCr-based high entropy alloy coatings: Effect of nitrogen additions on microstructural development, mechanical properties and tribological performance. *Appl. Surf. Sci.* **2020**, *507*, 145101. [CrossRef]
26. Jhong, Y.-S.; Huang, C.-W.; Lin, S.-J. Effects of CH4 flow ratio on the structure and properties of reactively sputtered (CrNbSiTiZr) Cx coatings. *Mater. Chem. Phys.* **2018**, *210*, 348–352. [CrossRef]
27. Braic, M.; Braic, V.; Balaceanu, M.; Zoita, C.N.; Vladescu, A.; Grigore, E. Characteristics of (TiAlCrNbY) C films deposited by reactive magnetron sputtering. *Surf. Coat. Technol.* **2010**, *204*, 12–13. [CrossRef]
28. Čekada, M.; Panjan, P.; Drnovšek, A.; Panjan, M.; Gselman, P. Growth defects in pvd hard coatings. In *Recent Advances in Thin Films*; Kumar, S., Aswal, D.K., Eds.; Springer: Singapore, 2020; pp. 35–73.
29. Bilek, M.M.M.; Martin, P.J.; McKenzie, D.R. Influence of gas pressure and cathode composition on ion energy distributions in filtered cathodic vacuum arcs. *J. Appl. Phys.* **1998**, *83*, 2965–2970. [CrossRef]